Constraints on ultracompact minihalos from the extragalactic gamma-ray background observation

Xing-Fu Zhang, Ji-Gui Cheng, Ben-Yang Zhu, Tian-Ci Liu, Yun-Feng Liang,* and En-Wei Liang†

Laboratory for Relativistic Astrophysics, Department of Physics, Guangxi University, Nanning 530004, China

(Received 23 September 2021; accepted 21 January 2022; published 17 February 2022)

Ultracompact minihalo (UCMH) is a special type of dark matter halo with a very steep density profile that may form in the early Universe seeded by an overdense region or a primordial black hole. Constraints on its abundance give valuable information on the power spectrum of primordial perturbation. In this work, we update the constraints on the UCMH abundance in the Universe using the extragalactic gamma-ray background observation. Comparing to previous works, we adopt the updated Fermi-LAT extragalactic gamma-ray background measurement and derive constraints based on a full consideration of the astrophysical contributions. With these improvements, we place constraints on UCMH abundance 1–2 orders of magnitude better than previous results. With the background components considered, we can also attempt to search for possible additional components beyond the known astrophysical contributions.

DOI: 10.1103/PhysRevD.105.043011

I. INTRODUCTION

The extragalactic gamma-ray background (EGB) is the total contribution of gamma-ray integrated flux from all objects in the history of the extragalactic Universe, and was first detected by the SAS-2 satellite [1,2] and subsequently measured by the Energetic Gamma Ray Experiment Telescope (EGRET) [3–5]. Better measurements on EGB were achieved by the Large Area Telescope (LAT) [6] instrument installed on the Fermi satellite [7,8]. The integrated flux of Fermi-LAT observation above 100 MeV is $1.29 \pm 0.07 \times 10^{-5}$ ph/cm^2/s/sr (Model B of [8]), consistent with those of EGRET, 1.14 ± 0.05 ph/cm^2/s/sr [9]. The latest Fermi-LAT observation shows that a power law function with an exponential cutoff $[dN/dE = I_{100}(E/100\ \mathrm{MeV})^{-\gamma}\exp(-E/E_{\mathrm{cut}})]$ can well describe the EGB spectrum [8] with a spectral index of $\gamma = 2.28 \pm 0.01$ and a cutoff energy of $E_{\mathrm{cut}} = 267 \pm 37$ GeV (model B of [8]).

Fermi-LAT also provides more accurate observations of extragalactic sources [10,11], allowing for a better understanding of the compositions of the EGB. It has been shown that the extragalactic gamma-ray background is mainly contributed by Blazars, radio galaxies (RGs), and star-forming galaxies (SFGs) [12–20]. Most of extragalactic sources detected in the Fermi sky are blazars [21], which can be further classified into two subclasses, BL Lacertae objects and flat-spectrum radio quasars [22]. Blazars could emit gamma rays through inverse Compton scattering (ICS) and/or hadronic processes and their contribution to EGB has been widely discussed [14,15,17–19]. Radio galaxies, although with lower gamma-ray luminosity for individual sources, are more numerous in the whole sky. The contribution of RGs to the EGB can be studied via the correlation between radio and gamma-ray luminosities [12,16]. The γ-ray radiation of SFGs arises from the decay of neutral mesons produced in the inelastic interaction of cosmic rays with the interstellar medium and interstellar radiation field [13,23]. Above 100 MeV, RGs and SFGs each contribute about 10–30% of the observed photon flux of EGB, while blazars contribute about ∼50% [17]. In addition, the contributions to EGB from other sources or processes include gamma-ray bursts (GRBs) [24], pulsars at high galactic latitudes [25], intergalactic shocks [26,27], cascade processes of high energy cosmic rays [28], and so on.

Except for the aforementioned components, another source that may contribute to EGB is dark matter (DM) [17,29–35]. The existence of DM has been confirmed by many astronomical and cosmological observations, and it is likely to account for ∼26% of the total energy density of the Universe [36]. DM has the potential to emit gamma-ray signals through annihilation or decay. The flux depends on the interaction cross section of DM particles and the DM abundance [37,38]. Therefore, the DM properties (cross section or abundance) can be constrained by requiring the expected flux not higher than the actual measurements of the EGB spectrum.

In this work, we will focus on a particular DM halo model, i.e., ultracompact minihalos (UCMH) [39–43], and constrain their abundance in the Universe with the EGB observation. The UCMH is characterized by a very steep

*liangyf@gxu.edu.cn
†lew@gxu.edu.cn

density profile ($\rho \propto r^{-9/4}$). If DM consists of weakly interacting massive particles (WIMPs), the UCMHs will be gamma-ray emitters due to the DM annihilation within them and the profile makes them have high expected gamma-ray flux compared to the normal DM halo [e.g., Navarro–Frenk–White (NFW) [44], Einasto [45]]. Constraints on the abundance of UCMHs or primordial black hole (PBHs) may provide valuable information on the power spectrum of the primordial perturbulation at small scale [46–49].

In idealized cases, the UCMH can form in the early Universe when the primordial density perturbations are between 10^{-3} and 0.3 (a PBH will be produced if the amplitude of the perturbation is $\delta > 0.3$ [50]). However it has been shown that the postulated steep inner profile cannot appear in realistic simulations since the required initial conditions (self-similarity, radial infall, isolation, etc.) for forming UCMHs can only be satisfied in idealized cases [51–53]. Alternatively, PBHs formed in the early Universe can accrete DM particles due to gravity and form UCMHs (a mixed WIMP-PBH dark matter model) [43,53]. In this work, we give constraints from an observational aspect, regardless of the exact mechanism of UCMH formation. Our constraints on the UCMH abundance can be directly converted into constraints on the PBHs in the mixed model [43]. Furthermore, the derived constraints are also valid for the minispike around a astrophysical black hole [54–57].

Comparing to previous works [41,43], our studies contain the following improvements. We use the updated Fermi-LAT EGB observation to perform the analysis. In addition, in the previous works of limiting the abundance of UCMH with the EGB observations [41,43,49], they usually used the inclusive energy spectrum to provide relatively conservative constraints without considering the astrophysical components. We will alternatively derive restrictions based on a full consideration of the astrophysical contributions to obtain more realistic (though not that conservative) results. With the background components considered, we can also attempt to search for possible signals/additional components beyond the background. Another motivation for our study of UCMH is that this type of objects was recently suggested to be able to better (compared to the traditional density profiles, e.g., NFW, Einasto) interpret the tentative 1.4 TeV e^+e^- excess of DAMPE (Dark Matter Particle Explorer) [56,58–60]. We therefore examine whether such a probability can accommodate the abundance upper limits derived from the EGB observation.

Through out this paper, we use the cosmological parameters from *Planck* 2015 [36], i.e., $\Omega_m = 0.31$, $\Omega_\Lambda = 0.69$, and $H_0 = 67.74\ \mathrm{km\,Mpc^{-1}\,s^{-1}}$.

II. METHOD

A. The model expected gamma-ray signal from a single UCMH

UCMHs are growing spherical DM halos, which are seeded by an overdense region in the early Universe with initial density perturbations greater than 0.01% (or alternatively seeded by a PBH). The mass of UCMHs M_u depends on their formation time and can be described as [39,40]

$$M_u(z) = \delta_m \left(\frac{1+z_{\rm eq}}{1+z}\right), \tag{1}$$

where δ_m is the mass of the perturbation at the redshift of matter-radiation equality ($1 + z_{\rm eq} \approx 3260$). Since the accretion will be prevented after $z = 10$, we assume the UCMHs stopped growing at $z = 10$, i.e., $M(z < 10) = M(z = 10)$ [40]. Compared to the amplitude of perturbations seen in cosmic microwave background (CMB) observation ($\sim 10^{-5}$), the required value for forming UCMH ($>10^{-3}$) is large. The non-Gaussian perturbations at phase transitions can enhance the amplitudes at a small scale, therefore the UCMHs are more likely born at the epoches of phase transitions. The UCMHs produced at three phase transitions are usually considered in literature [40–42,46]: electroweak symmetry breaking, the QCD confinement, and e^+e^- annihilation. The δ_m for (QCD, EW, e^+e^-) epoches are $\delta_{m,\{\rm EW,QCD,e^+e^-\}} = \{5.6\times10^{-19}, 1.1\times10^{-9}, 0.33\}\ \mathrm{M_\odot}$ [40] and the current masses of UCMHs are $M_u(0) = \{1.6\times10^{-7}, 0.2, 1.2\times10^{5}\}\ \mathrm{M_\odot}$, respectively. In fact, the chosen of the δ_m does not affect the predicted EGB spectrum of UCMH [41].

UCMHs are predicted to form by the secondary infall of DM onto PBHs or initial DM overdensity produced by the primordial density perturbation. The DM particles within the overdense region initially have an extremely small velocity dispersion. UCMHs thus form via a spherically symmetric gravitational collapse (pure radial infall). According to the secondary infall theory [61,62], the UCMHs will develop a self-similar power-law density profile $\rho \propto r^{-9/4}$. Such a steep profile is supported by both analytical solution [61,62] and (idealized) N-body simulations [51,63,64]. Normalizing the $\rho(r)$ to make it have a halo mass of $M_u(z)$ within the truncated radius $R_u(z)$ gives the density profile of [39,40]

$$\rho_u(r,z) = \frac{3 f_\chi M_u(z)}{16\pi R_u(z)^{3/4} r^{9/4}}, \tag{2}$$

where $f_\chi = \Omega_\chi/(\Omega_b + \Omega_\chi) \approx 0.83$ [36]. The profile truncated at a halo radius [40]

$$R_u(z) = 0.019 \left(\frac{1000}{z+1}\right)\left(\frac{M_u(z)}{\mathrm{M_\odot}}\right)^{1/3} \mathrm{pc}. \tag{3}$$

Due to the DM annihilation, for the most inner region of the halo ($r < r_{\rm cut}$) the density is set to [65]

$$\rho_{\rm max}(z) = \frac{m_\chi}{\langle\sigma v\rangle (t(z) - t_i)}, \tag{4}$$

where m_χ is the mass of DM particle, $\langle\sigma v\rangle$ the annihilation cross section, and $t(z)$ is the age of the Universe at redshift z. The $r_{\rm cut}$ is determined by requiring the $\rho_{\rm max} = \rho(r_{\rm cut})$.

If DM consists of WIMPs, then it can produce gamma rays through annihilation or decay. In this work, we are mainly concerned about the annihilation DM. The expected gamma-ray flux emitted from a single UCMH can be expressed as

$$F(E) = \frac{1}{4\pi}\frac{\langle\sigma v\rangle}{2m_\chi^2}\frac{dN_\gamma}{dE} \times \iint_{\rm los} \rho_u^2(r) ds d\Omega, \tag{5}$$

where dN_γ/dE is the photon yield per annihilation, which is calculated using PPPC4DMID [66].

B. Extragalactic γ-ray background from UCMHs

For UCMHs with monochromatic mass function, the differential EGB energy spectrum contributed by UCMHs is expressed as [43,65,67]

$$\frac{d\phi_\gamma}{dE} = \frac{f_u \rho_{c,0}}{M_u(0)}\frac{c}{8\pi}\frac{\langle\sigma v\rangle}{m_\chi^2}\int_0^{z_{\rm up}} dz \frac{e^{-\tau(E,z)}}{H(z)}\frac{dN_\gamma}{dE}(E',z) \times \int \rho_u^2(r,z) dV, \tag{6}$$

where f_u is the present abundance of UCMHs (in terms of the fraction of the critical density $\rho_{c,0}$), $E' = E(1+z)$ is the photon energy at redshift z, E is the observed photon energy, the $z_{\rm up} = m_\chi/E - 1$ is the maximal redshift that a UCMH can contribute of photons of energy E. For the DM annihilation cross section, we adopt the thermal relic value $\langle\sigma v\rangle = 3\times10^{-26}$ cm^3/s [68]; and for the Hubble parameter $H(z) = H_0\sqrt{\Omega_M(1+z)^3+\Omega_\Lambda}$, we use the cosmological parameters from *Planck* 2015 [36]. The $\tau(E,z)$ in Eq. (6) is the optical depth, for which we consider the extragalactic background light (EBL) absorption only, and can be approximated by $\tau(E,z) \sim z/3.3(E/10\ {\rm GeV})^{0.8}$ [67]. We use the approximation expression (rather than the models of, e.g., [69,70]) for better obtaining τ at high redshift (e.g., $z > 10$).

In addition to the prompt gamma-ray emission, DM annihilation can produce energetic electrons/positrons, which generate gamma rays through ICS off background radiation field. In this work, we only consider the prompt gamma rays from DM annihilation but neglecting the secondary IC component. Tighter constraints are expected with the IC contribution included. The contribution to the EGB from normal halos is also ignored, since it has been shown that the inclusion of them hardly affect the results [41] due to the much lower annihilation rate therein. For the three typical channels $b\bar{b}, \tau^+\tau^-$, and e^+e^-, we show the DM-induced EGB spectra with $f_u = 1$ in Fig. 1.

C. Astrophysical components of the extragalactic gamma-ray background

Compared with former researches on limiting UCMHs with EGB, one of the improvements we consider is the contribution to EGB from background astrophysical components. The previous works have shown that most of the EGB can be accounted for by the joint contributions of blazars (including both BL Lac objects and flat-spectrum radio quasars), RGs, and SFGs. Above 100 MeV RGs and SFGs each contribute about 10–30% of the observed photon flux of EGB, while blazars contribute ~50% [17]. The luminosity functions of these source populations can be derived from the resolved gamma-ray sources (for blazar) or from the relations between radio/infrared and gamma-ray luminosities (for SFGs and RGs). The contribution from the unresolved extragalactic sources can then

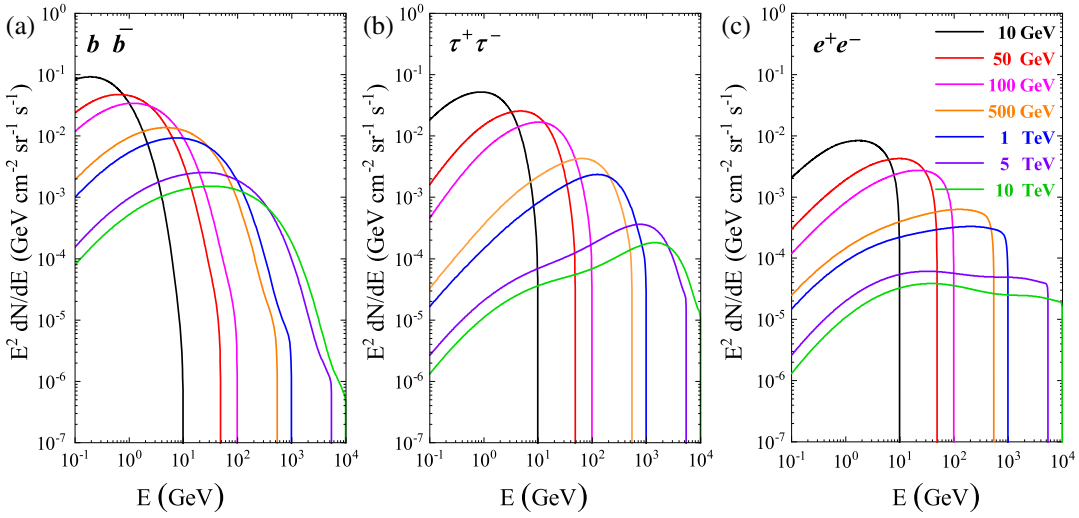

FIG. 1. The model-predicted EGB spectra from UCMHs ($f_u = 1$) for different channels and DM masses. The sharp cutoff at high energies close to M_χ could be a characteristic signature for DM search.

be estimated by extrapolating the luminosity function (LF). In this paper, we consider these three types of sources as well. For SFGs and RGs, we directly use the EGB spectrum (and corresponding uncertainties) presented in [13] (MW model) and [12]. A newer result for the SFG contribution to the EGB has been reported in [23]. We also use the SFG spectrum in [23] (the one based on the IR luminosity function of [71]) to test the main results of this paper and find that it only slightly affects the results since the SFG component accounts for merely 5% of the total EGB. For blazars we employ the formalism and parameters in [15,17], which will be briefly reintroduced below.

The differential intensity (in unit of ph cm^{-2} sr^{-1} s^{-1} × GeV^{-1}) of the EGB contributed by the blazars with photon index ($1.0 < \Gamma_\gamma < 3.5$), redshift ($10^{-3} < z < 6$), and gamma-ray luminosity ($10^{43} < L_\gamma < 10^{52}$) can be computed by

$$F_{\rm EGB}(E) = \int_{\Gamma_{\rm min}=1.0}^{\Gamma_{\rm max}=3.5} d\Gamma \int_{z_{\rm min}=10^{-3}}^{z_{\rm max}=6} dz \int_{L_{\gamma,\rm min}=10^{43}}^{L_{\gamma,\rm max}=10^{52}} dL_\gamma \times \Phi(L_\gamma, z, \Gamma) \cdot f(E) \cdot \frac{dV}{dz d\Omega}, \quad (7)$$

where $dV/(dzd\Omega)$ is the differential comoving volume at redshift z, and the EBL modulated spectrum of blazars is

$$f(E;\Gamma,z,L_\gamma) = K\left[\left(\frac{E}{E_b}\right)^{1.7} + \left(\frac{E}{E_b}\right)^{2.6}\right]^{-1} \cdot e^{-\tau(E,z)},$$

with $\log E_b(\mathrm{GeV}) \approx 9.25 - 4.11\Gamma$ and $K = L_\gamma/[4\pi d_L^2 k \times \int E f(E, K=1) dE]$, where k is the K-correction term. For the optical depth term here we use the EBL model of [69].

The Φ in Eq. (7) is the blazar LF, namely the number density of blazars at luminosity L_γ, redshift z and spectral index Γ. We use the simplest pure density evolution model of the LF, which reads

$$\Phi(L_\gamma, z, \Gamma) = \Phi(L_\gamma, z=0, \Gamma) \times e(z, L_\gamma), \quad (8)$$

where the luminosity function at redshift $z = 0$ is

$$\Phi(L_\gamma, z=0, \Gamma) = \frac{dN}{dL_\gamma dV d\Gamma}, = \frac{A}{\ln(10) L_\gamma}\left[\left(\frac{L_\gamma}{L_*}\right)^{\gamma_1} + \left(\frac{L_\gamma}{L_*}\right)^{\gamma_2}\right]^{-1} \cdot e^{-0.5[\Gamma-\mu(L_\gamma)]^2/\sigma^2}. \quad (9)$$

The expressions of $e(z, L_\gamma)$ and $\mu(L_\gamma)$ can be found in [17].

We plot the model expected EGB spectra for blazar, RG, and SFG together with the Fermi-LAT EGB measurements in Fig. 2. Also shown is the proportion of each component in the total observed EGB.

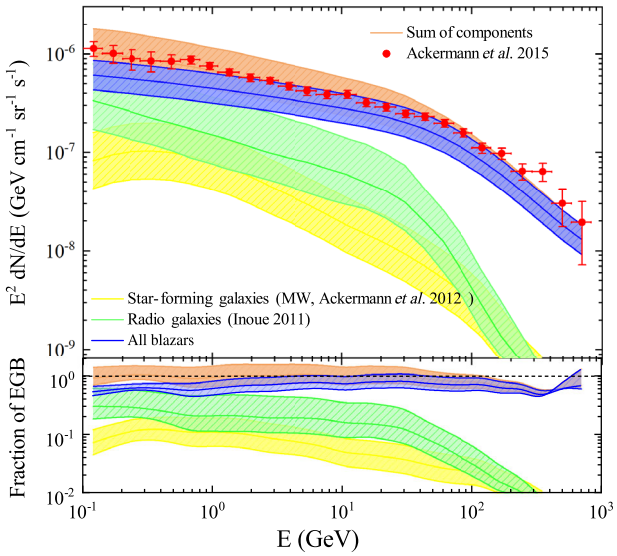

FIG. 2. The EGB spectrum observed by Fermi-LAT (red points) [8] together with the predicted astrophysical contributions from blazars (blue band) [17], radio galaxies (green band) [12], and star-forming galaxies (yellow band) [13]. All the components have not been renormalized through the χ^2 fitting, yet. The red band is the sum of all three components. The lower panel demonstrates the fraction of each astrophysical component contributing to the total EGB spectrum.

D. Limiting the abundance of UCMHs with the Fermi-LAT EGB observation

If the UCMHs exist in the Universe, then they are another type of extragalactic gamma-ray emitters due to the DM annihilation [40]. The annihilation photons may contribute to the extragalactic gamma-ray background, it is practicable to limit the abundance of UCMHs with EGB observation. The latest EGB measurements at GeV energies are from the Fermi-LAT observation [8]. The Fermi-LAT Collaboration adopted three different Galactic foreground models to obtain the EGB spectrum. For our purpose they do not differ with each other significantly, and in this paper we use the foreground model B of [8].

To compare the models with the observation, the χ^2 fitting method is used. We first obtain the best-fit astrophysical components without the DM model included by minimizing

$$\chi^2 = \sum_{i=1}^{N} \frac{(F_{i,\rm obs} - \boldsymbol{\alpha}_1 F_{i,1} - \boldsymbol{\alpha}_2 F_{i,2} - \boldsymbol{\alpha}_3 F_{i,3})^2}{\sigma_{i,\rm obs}^2} + \sum_{j=1}^{3} \frac{(1-\boldsymbol{\alpha}_i)^2}{\delta_j^2}, \quad (10)$$

where $F_{i,\rm obs}$ and the $\sigma_{i,\rm obs}$ are the EGB spectrum measured by the Fermi-LAT (see Table 3 of [8]). The error bars $\sigma_{i,\rm obs}$ include the statistical uncertainty and systematic

TABLE I. Best-fit results for the models with only astrophysical components.

Model[a]	Blazar	RG	SFG	χ^2
Benchmark	$1.146^{+0.031}_{-0.031}$	$0.621^{+0.125}_{-0.125}$	$1.202^{+0.251}_{-0.251}$	19.359
MAGN	$1.001^{+0.029}_{-0.029}$	$0.723^{+0.091}_{-0.091}$	$1.489^{+0.251}_{-0.251}$	19.785
RG($\Gamma = 2.11$)	$1.165^{+0.037}_{-0.037}$	$0.521^{+0.101}_{-0.101}$	$1.453^{+0.251}_{-0.251}$	24.288
SFG(PL)	$1.165^{+0.044}_{-0.044}$	$1.027^{+0.121}_{-0.121}$	$1.237^{+0.180}_{-0.180}$	19.558
SFG2020	$0.983^{+0.046}_{-0.046}$	$0.824^{+0.152}_{-0.152}$	$1.022^{+0.143}_{-0.143}$	21.685
$\tau = 1.49$	$0.964^{+0.004}_{-0.004}$	$1.840^{+0.153}_{-0.153}$	$1.417^{+0.251}_{-0.251}$	11.443
$\gamma_2 = 1.35$	$0.710^{+0.018}_{-0.018}$	$1.180^{+0.127}_{-0.127}$	$1.309^{+0.251}_{-0.251}$	12.772

[a]See Sec. IV A for the description of the tested models.

uncertainties from the effective area parameterization, as well as the cosmic-ray (CR) background subtraction [8]. The systematic uncertainty related to the modeling of the Galactic foreground is not further included, which may vary the intensity by $+15\%/-30\%$. However, we adopt the EGB spectrum having the highest intensities among the three benchmark foreground models in [8] [i.e., the foreground (FG) model B], which would give relatively conservative constraints. The $F_{i,1}$, $F_{i,2}$, $F_{i,3}$ in Eq. (10) are the model-expected fluxes of the ith energy bin from blazars, RGs, and SFGs, respectively, and the $\boldsymbol{\alpha}_i$ is a renormalization constant of each spectrum, which is free to vary in the fit. The last term is introduced to ensure that the best-fit gamma-ray intensities do not deviate from their original values in the literature too much. The δ_j is determined by the uncertainty band of each component as demonstrated in Fig. 2 and we choose a mean value over all the energies.

Based on the best-fit astrophysical model, we add an additional UCMH component into the χ^2 fit to constrain the UCMH abundance or search for possible signals. At this stage, the χ^2 is defined as

$$\chi^2 = \sum_{i=1}^{N} \frac{[F_{i,\mathrm{obs}} - \mathcal{A}F_{i,\mathrm{astro}} - f_u F_{i,\mathrm{UCMH}}]^2}{\sigma^2_{i,\mathrm{obs}}}, \quad (11)$$

where $F_{i,\mathrm{astro}}$ is the sum of the best-fit astrophysical contributions in the above step, and $F_{i,\mathrm{UCMH}}$ is the flux from UCMHs as calculated by Eq. (6).

The best-fit chi-square value $\chi^2_{f_u}$ will change along with the given normalization parameter of the UCMH component. The chi-square difference is $\Delta\chi^2 = \chi^2_{f_u} - \chi^2_{f_u=0}$, where $\chi^2_{f_u=0}$ is the minimum χ^2 under the background-only model. Because, for a fixed DM mass M_χ, the UCMH model has 1 more additional parameter than the background model, the chi-square difference follows $\Delta\chi^2 \sim \chi^2(1)$ [72]. The variance of the χ^2 by 2.71 corresponds to an upper limit of the abundance at a 95% confidence level.

III. RESULT

The fitted renormalization parameters α_i for the three background components and the 1σ uncertainties are summarized in Table I (benchmark row). For blazars and SFGs they are close to 1, while for RG a smaller renormalization parameter is required to fit the data. In Fig. 3 we exhibit the best-fit background-only EGB spectrum as well as the corresponding conservative residuals (see below). Also shown are the spectra of UCMH with $M_\chi = 1$ TeV in different annihilation channels, which are required not to exceed the residuals in the plot. We can see that,

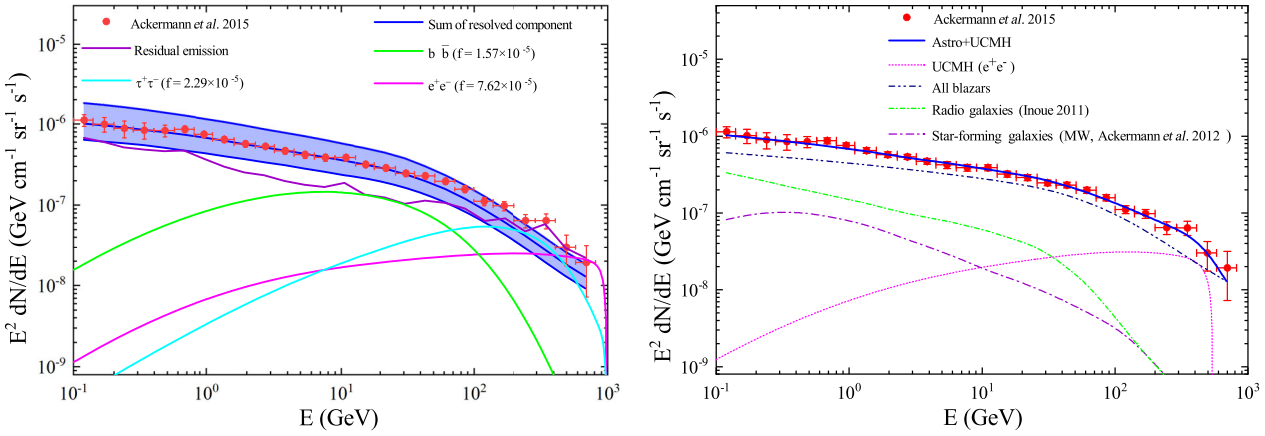

FIG. 3. Left panel: the best-fit EGB spectrum without a DM component included (blue line and relevant uncertainty band). The purple line is the conservative residuals subtracting the best-fit astrophysical contributions (see the main text for details). Also shown are the DM spectra for 1 TeV DM for $b\bar{b}$ (green line), $\tau^+\tau^-$ (cyan line), and e^+e^- (magenta line) channels, respectively. In this plot, the amplitude of the three components are determined by requiring not to exceed the residual emission (i.e., a demonstration of our conservative methods). Right panel: the best-fit total EGB spectrum containing the DM component (blue line) and the individual contributions.

below 50 GeV, the model matches the data points well, while at energies of >50 GeV, it slightly underestimates the observation.

According to the χ^2 analysis [Eq. (11)], the upper limits on the UCMH abundance f_u as a function of DM mass M_χ after containing astrophysical components in the fit are shown in Fig. 4 for $b\bar{b}$, $\tau^+\tau^-$, e^+e^- channels. For all three channels, we can place constraints on the abundance down to $\sim 3\times 10^{-6}$ in the range $M_\chi < 100$ GeV, namely only $\lesssim 3\times 10^{-6}$ of the Universe energy density could be in the form of UCMH, otherwise their predicted EGB emission will exceed the actual observation. For the $\tau^+\tau^-$ and e^+e^- channels, the constraints become weaker as the M_χ is increased to >300 GeV. This is due to the existence of residuals at this high energy range (see Fig. (11), which may be accounted for by including a DM component (see Sec. IV A).

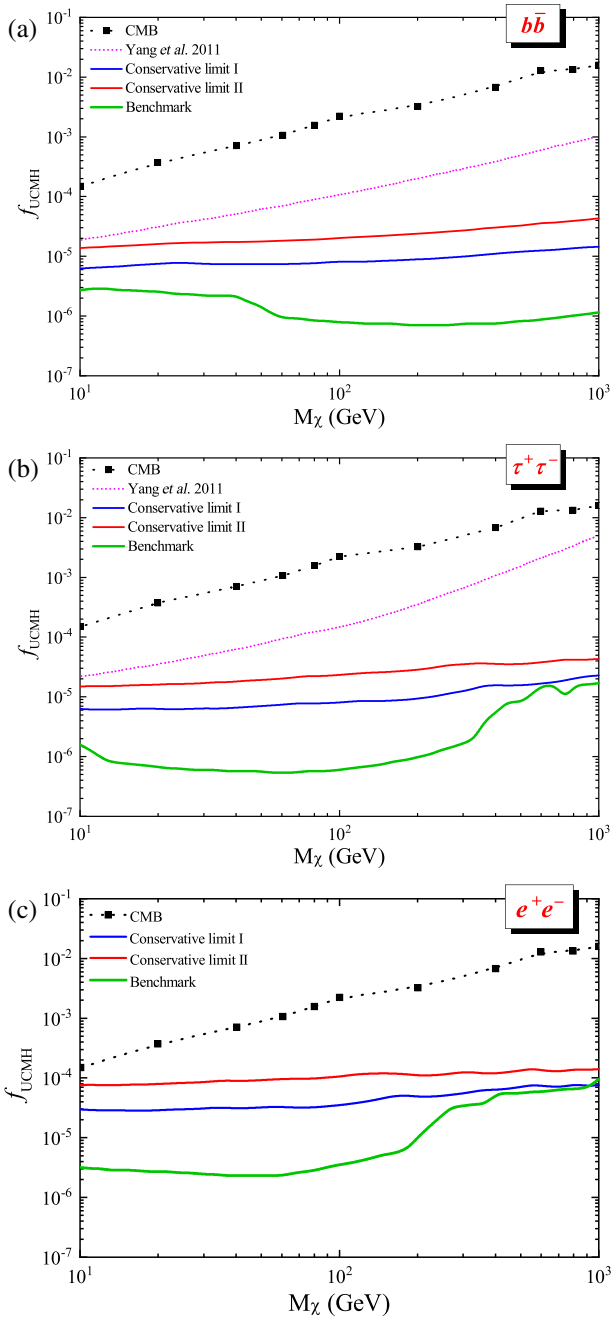

FIG. 4. The constraints on the UCMH abundance in the Universe obtained through the EGB analysis in this work (solid lines). As a comparison, we also plot the previous constraints based on EGB (dashed) and CMB (dotted) observations [41]. The three panels are for different annihilation channels as labeled in the plots.

Compared with the previous results which are based on the 1-year Fermi-LAT EGB observation [41] (dashed line in Fig. 4), we can see that our constraints are about 1–2 orders of magnitude better. The improvement is owing to the use of the updated EGB observation and subtracting the astrophysical contributions. The UCMH abundance f_u in the Universe can also be constrained by the CMB observation since in the early Universe the particles emitted from the DM annihilation within UCMHs will influence the ionization and recombination before the structure formation [41,42]. As a comparison, the CMB constraints with WMAP-7 data [41] are shown in the Fig. 4 (dotted line), which is however not as stringent as the EGB limits.

In addition, we use two other approaches to set more conservative limits. The most conservative one is obtained by using an inclusive EGB spectrum without any background subtracted (I). Less conservative limits (II) are given by the following prescription. We define the upper bound of the error bars of the EGB measurements as $F_{i,\mathrm{up}}$, while for the model we use the lower bound of the uncertainty bands $F_{i,\mathrm{low}}$, and $F_{i,\mathrm{res}} = F_{i,\mathrm{up}} - F_{i,\mathrm{low}}$ is considered a conservative residual after subtracting the background. Namely, for the observation we adopt the maximal values under the 1σ range, and for the model-expected one we use the minimum. Requiring that the EGB from UCMHs does not exceed the $F_{i,\mathrm{res}}$ gives the limits on the UCMH abundance. As is shown, even with the most conservative approach, the results are much better than [41], mainly due to the adoption of the new EGB observation.

IV. DISCUSSIONS

A. Search for possible additional DM component

In contrast with previous analyses, we are able to search for possible UCMH signals in addition to the background components because the astrophysical contributions are considered in this work. The search is also based on the chi-square analysis of Eq. (11). A background model corresponds to $f_u = 0$, while for the signal model f_u is free to vary. Then the significance of the existence of a UCMH component is given by the chi-square difference $\Delta\chi^2$. According to Wilks's theorem [72], the $\Delta\chi^2 > 9$ indicates the observed data rejecting the null model at a confidence level of $>3\sigma$; i.e., there may exist a possible signal.

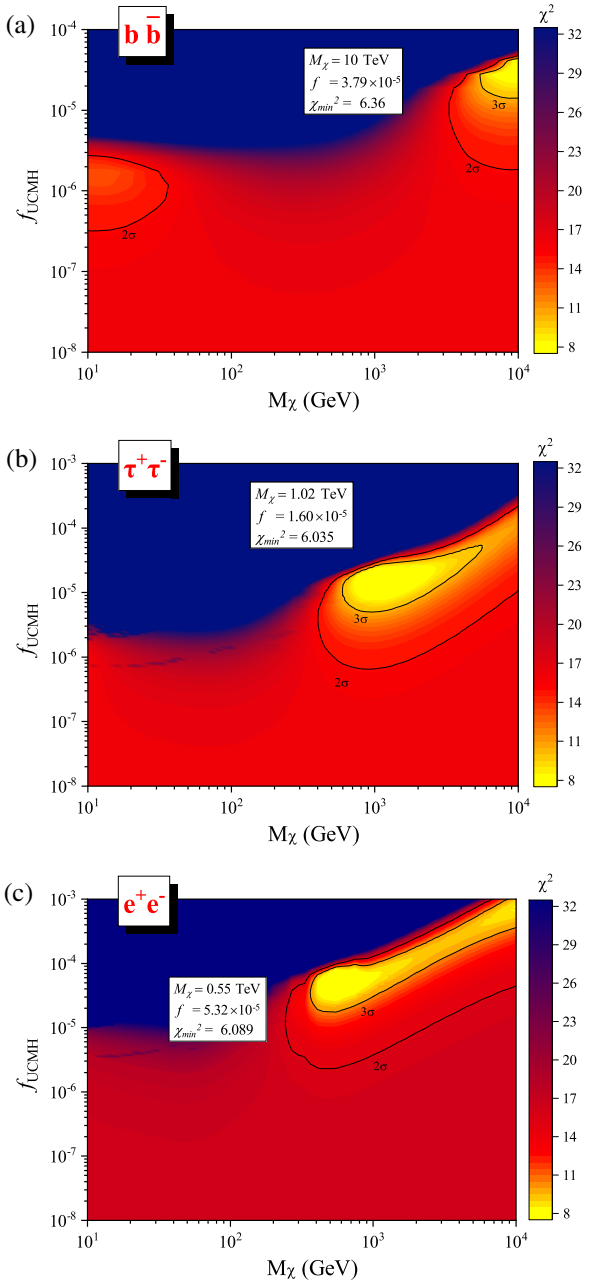

FIG. 5. The χ^2 maps as a function DM mass M_χ and UCMH abundance f_u for three different annihilation channels. The brightest point with minimum χ^2 corresponds to the best fit to the observation and the fitted parameters have been shown in the plots.

We scan for a series of DM masses with the EGB observation, and the related results are shown in Fig. 5.

In our analysis, we notice that the inclusion of a UCMH component improves the fit significantly. The test statistic (TS) of the additional DM composition can be estimated by the difference of the minimum chi-square values between the following two cases: the fitting of only considering the astrophysical components, and that with the addition of a UCMH composition, namely $\mathrm{TS} = \Delta\chi^2 = \tilde{\chi}^2(f_u = 0) - \tilde{\chi}^2$.

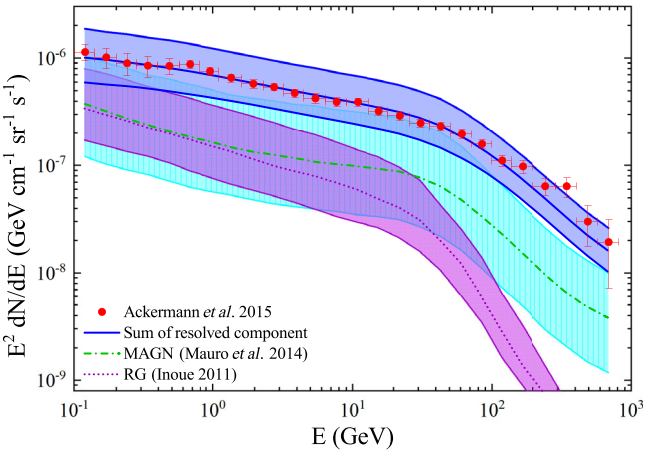

FIG. 6. We compare the RG models of [12,16]. The RG model from [12] has a higher EGB flux at higher energies. The blue line is the best fit adopting the model of [16] (DM component is not included).

The χ^2 with tilde denotes the minimum value in the fit. The brightest points in Fig. 5 give the best-fit M_χ and f_u parameters. We obtain the optimum DM masses of 10,[1] 1.09, and 0.55 TeV with TS of 13.0, 13.3, and 13.3 for $b\bar{b}$, $\tau\tau$, and e^+e^-, respectively. The TS > 9 suggests existing a tentative signal.

Although such a tentative excess is interesting, it is difficult to reliably claim that it comes from UCMHs, given the large uncertainties in the modeling of astrophysical components. We here demonstrate that the uncertainties in the astrophysical models have a great impact on the obtained significance. We note that the fitting is improved mainly because the addition of a UCMH component compensates for the residuals in the high energy range (see Fig. 3 right for the demonstration). In light of this, we focus on some alternative models that can increase the high energy flux of the EGB spectrum. We do the following checks.

The reference [31] has also searched for a probable DM component that could be hidden beneath the EGB. We note that they did not report the presence of a tentative additional component in the >100 GeV energy range.[2] One difference between their work and ours is that for the RG component, they employ the energy spectrum of [16] instead of [12] in our study. By comparison (Fig. 6), it can be found that the RG spectrum predicted by [16] (we denote it as MAGN model, where the acronym MAGN represents misaligned active galactic nuclei) has a higher energy flux than [12] at energies greater than 100 GeV. We use the RG model of [16] to check our results with the models of the other components

[1]The 10 TeV is the upper boundary of the scanned M_χ.

[2]Note that they focused on the DM halo of the Milky Way rather than the extragalactic UCMHs here. However if the additional UCMH component does exists, it will be partly revealed in their results since both (UCMH and MW halo) spectra have more or less similar bumplike shape.

TABLE II. Best-fit parameters for the models with DM included.

Model	Channel	f_u	M_χ[a]	TS[b]	χ^2
Benchmark	$b\bar{b}$	3.79×10^{-5}	10	12.99	6.36
Benchmark	$\tau^+\tau^-$	1.60×10^{-5}	1.09	13.32	6.03
Benchmark	e^+e^-	5.23×10^{-5}	0.55	13.27	6.08
MAGN	$\tau^+\tau^-$	1.50×10^{-5}	1.48	12.69	7.09
RG/$\Gamma = 2.11$	$\tau^+\tau^-$	1.45×10^{-5}	1.48	14.78	9.50
SFG/PL	$\tau^+\tau^-$	1.85×10^{-5}	1.35	11.44	7.91
SFG2020	$\tau^+\tau^-$	1.87×10^{-5}	1.23	14.56	7.12
$\tau = 1.49$	$\tau^+\tau^-$	1.17×10^{-5}	1.66	5.27	6.17
$\gamma_2 = 1.35$	$\tau^+\tau^-$	3.94×10^{-6}	2.23	5.05	7.72

[a]DM mass in unit of TeV.
[b]TS value of the UCMH component.

unchanged. The results reveal that even when the RG model is replaced, the fitting still gives a relatively high TS of the tentative DM component (see MAGN model in Tables I and II).

In addition, when modeling the SFG component, different assumptions of the average spectrum of the source population will lead to different EGB spectra of SFGs [13]. Our benchmark results adopt the MW model (i.e., assuming all SFGs are Milky Way–like), but at 100 GeV the PL model (all SFGs share the same power-law spectrum as those detected by Fermi-LAT) is higher than the MW model by a factor of ∼10. We therefore examine the outcome of taking this SFG/PL model. Further, we notice that an updated result for the SFG contribution to the EGB has been reported in [23]. They derive the SFG spectrum based on the detection of 11 SFGs and the emission from unresolved SFGs with the 10-year Fermi-LAT data. We test the analysis with this SFG model and find results consistent with our benchmark ones. The related results are shown in the SFG2020 row of the two tables.

The large uncertainties in the LF parameters will induce a significant uncertainty of the predicted EGB spectrum. For RG we examine the spectral uncertainty introduced by the photon index parameter. We consider a harder photon index ($\Gamma = 2.11$) of the source population in the luminosity function (see Fig. 4 of [12]). The corresponding results are shown in Tables I and II (labeled as RG/$\Gamma = 2.11$). For the blazar component, with the formalism described in Sec. II C, we test the uncertainties associated with all 10 parameters of the pure density evolution LF. The τ and γ_2 parameters are found to have the greatest influence on the obtained TS value when the parameter values are changed within their uncertainty range. The TS reduces to ∼5.3 and ∼5.1 for the $\tau = 1.49$ and $\gamma_2 = 1.35$ models, respectively.

According to these test, we conclude that the results from the EGB analysis are currently subject to considerable uncertainty and we can not claim the presence of additional components despite obtaining a relatively high TS value.

B. The UCMH contribution to the e^+e^- energy density near the Earth

At last we discuss the implication of our constraints to the DAMPE 1.4 TeV excess. One of the most intriguing structure displayed in the DAMPE e^+e^- spectrum is the peaklike excess at ∼1.4 TeV with a significance of $\sim 3.7\sigma$, which may be caused by the monochromatic injection of electrons due to the DM annihilation within nearby DM halos [58–60,73–75]. In the DM scenario, the DM annihilation is accompanied with production of gamma-ray photons. While the normal DM halo models (like NFW [44], Einasto [45]) are challenged by the gamma-ray observations [76,77], the DM annihilation within nearby UCMHs can provide a better interpretation to the excess [56,59,60]. Assuming that the local fraction of the DM in the form of UCMHs is identical to that in the whole Universe, the above constraints can be used to examine the UCMH interpretation of the 1.4 TeV excess.

Here we especially consider the channel of $\chi\chi \to e^+e^-$. The number of electrons/positrons emitted per unit time and energy from a UCMH is

$$\frac{dN_e}{dEdt} = 2R \cdot \delta(E - E'), \tag{12}$$

with R the annihilation rate of the DM particles within the UCMH

$$R = \frac{\langle \sigma v \rangle}{2m_\chi^2} \int \rho^2 \mathrm{d}V. \tag{13}$$

We then have the injection rate of

$$Q(E, r) = \frac{f_u \rho_{\chi,\mathrm{local}}}{M_u(0)} \frac{dN_e}{dEdt}, \tag{14}$$

where $\rho_{\chi,\mathrm{local}} = 0.4\ \mathrm{GeV/cm^3}$ [78] is the DM density near the location of the Earth. By solving the propagation equation of electrons one can obtain the energy density ω_e contributed by UCMHs for a given f_u. The narrow peak of the tentative excess requires the distance of the source is within $d = 0.3$ kpc for avoiding the broadening of the peak due to cooling effect [59,73]. Assuming the DM density of the field halo does not vary a lot within the region of propagation length (i.e., assuming the UCMHs distributed evenly near the Earth), we can reasonably neglect the diffusion term, and the number density of the electrons provided by UCMHs can be approximated by

$$\frac{dn_e}{dE} = \frac{1}{b(E)} \int_E^\infty Q(E', r) dE', \tag{15}$$

where the $b(E) \approx b_2(E/\mathrm{GeV})^2$ is the electron cooling rate, for which we consider only the synchrotron and ICS losses $b_2 = 1.0 \times 10^{-16}$ GeV/s [73,79].

The measured energy density of the 1.4 TeV peak is estimated to be about 1.2×10^{-18} erg cm^{-3} [73]. However, using Eq. (15) and the upper limits of the UCMH abundance in Fig. 4, we obtain an upper limits of the energy density of $\omega_{\mathrm{up}} \sim 6.25 \times 10^{-19}$ erg/cm^3 for the e^+e^- channel. This indicates that the UCMHs formed in the transition epoches with a density profile of $\gamma = -9/4$ is hard to interpret the DAMPE 1.4 TeV excess if the UCMH abundance near the Earth is the same as that in the whole Universe. It has also been shown that such type ($\gamma = -9/4$) of UCMH is not supported by the realistic simulations [51–53]. To still use UCMH to account for the 1.4 TeV excess, possible solution is that the UCMHs are in the form of $\gamma = -3/2$ as expected by the simulations. The shallower density profile reduces the annihilation rate in the UCMHs, making the upper limits of the abundance deduced from the EGB observation much weaker. Note that the $\gamma = -3/2$ UCMHs could also behave as pointlike sources in the Fermi-LAT gamma-ray sky [56], and would not be constrained by the gamma-ray observation. Another possibility is the UCMH abundance near the Earth is higher than the average value in the whole Universe.

V. SUMMARY

In this work, we revisit the analysis of constraining the UCMH abundance with EGB observations, using the latest measurements at 0.1–820 GeV energies by Fermi-LAT. Except for the use of updated data, another improvement of this work is that we take into account the astrophysical contributions in the EGB and subtract them before setting the constraints in order to obtain more strict limits on the abundance. With these improvements, we find that our results are 1–2 orders of magnitude better than previous. Even adopting a conservative method of using the inclusive EGB spectrum as [41], our results are substantially stronger due to the use of the new EGB observation [8]. Thus, the constraints presented in the work are currently the most serious ones for the UCMHs with monochromatic mass function. Though some N-body simulations do not support the existence of UCMHs, our results can also apply to the dressed PBH [43,53].

In addition to deriving constraints, we also search for possible DM components after subtracting the astrophysical contributions. We find that in our benchmark model (see Table II), the χ^2 analysis shows that the significance of existing a UCMH component reaches 3.6σ (i.e., TS = 13.3) for the $\tau^+\tau^-$ channel. For $b\bar{b}$ and e^+e^-, the TS values are 13.0 and 13.3, respectively. However, we point out that the uncertainty of the astrophysical models is large and it is hard to claim the existence of an additional component at present. The TS value can be reduced to as low as ∼5.3 if we change the astrophysical models. Observing more resolved extragalactic sources in the future with next generation gamma-ray telescopes (especially for the SFG and RG components) will be helpful to better determine the gamma-ray luminosity function of these source classes and is crucial for the better determination of whether existing additional components in the EGB.

ACKNOWLEDGMENTS

We thank the kindly suggestion from the anonymous referee. We thank Yupeng Yang and Houdun Zeng for their helpful discussions. This work is supported by the National Natural Science Foundation of China (Grants No. 11851304, No. U1738136, No. 11533003, No. U1938106, and No. 11703094) and the Guangxi Science Foundation (Grants No. 2017AD22006, No. 2019AC20334, and No. 2018GXNSFDA281033) and Bagui Young Scholars Program (LHJ).

[1] C. E. Fichtel, G. A. Simpson, and D. J. Thompson, Diffuse gamma radiation, Astrophys. J. **222**, 833 (1978).
[2] D. J. Thompson and C. E. Fichtel, Extragalactic gamma radiation—Use of galaxy counts as a galactic tracer, Astron. Astrophys. **109**, 352 (1982).
[3] J. L. Osborne, A. W. Wolfendale, and L. Zhang, The diffuse flux of energetic extragalactic gamma rays, J. Phys. G Nucl. Phys. **20**, 1089 (1994).
[4] P. Sreekumar *et al.*, EGRET observations of the extragalactic gamma-ray emission, Astrophys. J. **494**, 523 (1998).
[5] T. D. Willis, Observations of the isotropic diffuse gamma-ray background with the EGRET telescope, Ph.D. Thesis, arXiv:astro-ph/0201515.
[6] W. B. Atwood *et al.*, The large area telescope on the Fermi gamma-ray space telescope mission, Astrophys. J. **697**, 1071 (2009).
[7] A. A. Abdo *et al.*, Spectrum of the Isotropic Diffuse Gamma-Ray Emission Derived from First-Year Fermi Large Area Telescope Data, Phys. Rev. Lett. **104**, 101101 (2010).
[8] M. Ackermann *et al.*, The spectrum of isotropic diffuse gamma-ray emission between 100 MeV and 820 GeV, Astrophys. J. **799**, 86 (2015).
[9] A. W. Strong, I. V. Moskalenko, and O. Reimer, A new determination of the extragalactic diffuse gamma-ray background from EGRET data, Astrophys. J. **613**, 956 (2004).

[10] F. Acero *et al.*, Fermi large area telescope third source catalog, Astrophys. J. Suppl. Ser. **218**, 23 (2015).
[11] S. Abdollahi *et al.*, Fermi large area telescope fourth source catalog, Astrophys. J. Suppl. Ser. **247**, 33 (2020).
[12] Y. Inoue, Contribution of gamma-ray-loud radio galaxies' core emissions to the Cosmic MeV and GeV gamma-ray background radiation, Astrophys. J. **733**, 66 (2011).
[13] M. Ackermann *et al.*, GeV observations of star-forming galaxies with the Fermi large area telescope, Astrophys. J. **755**, 164 (2012).
[14] H. Zeng, D. Yan, and L. Zhang, A revisit of gamma-ray luminosity function and contribution to the extragalactic diffuse gamma-ray background for Fermi FSRQs, Mon. Not. R. Astron. Soc. **431**, 997 (2013).
[15] M. Ajello *et al.*, The cosmic evolution of Fermi BL Lacertae objects, Astrophys. J. **780**, 73 (2014).
[16] M. Di Mauro, F. Calore, F. Donato, M. Ajello, and L. Latronico, Diffuse γ-ray emission from misaligned active galactic nuclei, Astrophys. J. **780**, 161 (2014).
[17] M. Ajello *et al.*, The origin of the extragalactic gamma-ray background and implications for dark matter annihilation, Astrophys. J. **800**, L27 (2015).
[18] Y. Qu, H. Zeng, and D. Yan, Gamma-ray luminosity function of BL Lac objects and contribution to the extragalactic gamma-ray background, Mon. Not. R. Astron. Soc. **490**, 758 (2019).
[19] H. Zeng, V. Petrosian, and T. Yi, Cosmological evolution of Fermi large area telescope gamma-ray blazars using novel nonparametric methods, Astrophys. J. **913**, 120 (2021).
[20] M. A. Roth, M. R. Krumholz, R. M. Crocker, and S. Celli, The diffuse γ-ray background is dominated by star-forming galaxies, Nature (London) **597**, 341 (2021).
[21] M. Ajello *et al.*, The fourth catalog of active galactic nuclei detected by the Fermi large area telescope, Astrophys. J. **892**, 105 (2020).
[22] P. Padovani, Unified schemes for radio-loud AGN: Recent results, Mem. Soc. Astron. Ital. **68**, 47 (1997).
[23] M. Ajello, M. Di Mauro, V. S. Paliya, and S. Garrappa, The γ-ray emission of star-forming galaxies, Astrophys. J. **894**, 88 (2020).
[24] S. Casanova, B. L. Dingus, and B. Zhang, Contribution of GRB emission to the GeV extragalactic diffuse gamma-ray Flux, Astrophys. J. **656**, 306 (2007).
[25] C.-A. Faucher-Giguère and A. Loeb, The pulsar contribution to the gamma-ray background, J. Cosmol. Astropart. Phys. 01 (2010) 005.
[26] A. Loeb and E. Waxman, Cosmic γ-ray background from structure formation in the intergalactic medium, Nature (London) **405**, 156 (2000).
[27] T. Totani and T. Kitayama, Forming clusters of galaxies as the origin of unidentified GEV gamma-ray sources, Astrophys. J. **545**, 572 (2000).
[28] A. Dar and N. J. Shaviv, Origin of the High Energy Extragalactic Diffuse Gamma Ray Background, Phys. Rev. Lett. **75**, 3052 (1995).
[29] K. N. Abazajian, P. Agrawal, Z. Chacko, and C. Kilic, Conservative constraints on dark matter from the Fermi-LAT isotropic diffuse gamma-ray background spectrum, J. Cosmol. Astropart. Phys. 11 (2010) 041.
[30] S. Ando and K. Ishiwata, Constraints on decaying dark matter from the extragalactic gamma-ray background, J. Cosmol. Astropart. Phys. 05 (2015) 024.
[31] M. Di Mauro and F. Donato, Composition of the Fermi-LAT isotropic gamma-ray background intensity: Emission from extragalactic point sources and dark matter annihilations, Phys. Rev. D **91**, 123001 (2015).
[32] Fermi LAT Collaboration, Limits on dark matter annihilation signals from the Fermi LAT 4-year measurement of the isotropic gamma-ray background, J. Cosmol. Astropart. Phys. 09 (2015) 008.
[33] W. Liu, X.-J. Bi, S.-J. Lin, and P.-F. Yin, Constraints on dark matter annihilation and decay from the isotropic gamma-ray background, Chin. Phys. C **41**, 045104 (2017).
[34] C. Blanco and D. Hooper, Constraints on decaying dark matter from the isotropic gamma-ray background, J. Cosmol. Astropart. Phys. 03 (2019) 019.
[35] A. Arbey, J. Auffinger, and J. Silk, Constraining primordial black hole masses with the isotropic gamma ray background, Phys. Rev. D **101**, 023010 (2020).
[36] P. A. R. Ade *et al.* (Planck Collaboration), Planck 2015 results. XIII. Cosmological parameters, Astron. Astrophys. **594**, A13 (2016).
[37] K. Belotsky, A. Kirillov, and M. Khlopov, Gamma-ray evidence for dark matter clumps, Gravitation Cosmol. **20**, 47 (2014).
[38] K. Belotsky, M. Khlopov, and A. Kirillov, Gamma-ray effects of dark forces in dark matter clumps, arXiv:1312.6853.
[39] M. Ricotti and A. Gould, A new probe of dark matter and high-energy universe using microlensing, Astrophys. J. **707**, 979 (2009).
[40] P. Scott and S. Sivertsson, Gamma Rays from Ultracompact Primordial Dark Matter Minihalos, Phys. Rev. Lett. **103**, 211301 (2009).
[41] Y. Yang, L. Feng, X. Huang, X. Chen, T. Lu, and H. Zong, Constraints on ultracompact minihalos from extragalactic γ-ray background, J. Cosmol. Astropart. Phys. 12 (2011) 020.
[42] Y. Yang, X. Huang, X. Chen, and H. Zong, New constraints on primordial minihalo abundance using cosmic microwave background observations, Phys. Rev. D **84**, 043506 (2011).
[43] Y. Yang, The abundance of primordial black holes from the global 21 cm signal and extragalactic gamma-ray background, Eur. Phys. J. Plus **135**, 690 (2020).
[44] J. F. Navarro, C. S. Frenk, and S. D. M. White, A universal density profile from hierarchical clustering, Astrophys. J. **490**, 493 (1997).
[45] V. Springel, J. Wang, M. Vogelsberger, A. Ludlow, A. Jenkins, A. Helmi, J. F. Navarro, C. S. Frenk, and S. D. M. White, The Aquarius project: The subhaloes of galactic haloes, Mon. Not. R. Astron. Soc. **391**, 1685 (2008).
[46] A. S. Josan and A. M. Green, Gamma rays from ultracompact minihalos: Potential constraints on the primordial curvature perturbation, Phys. Rev. D **82**, 083527 (2010).
[47] T. Bringmann, P. Scott, and Y. Akrami, Improved constraints on the primordial power spectrum at small scales from ultracompact minihalos, Phys. Rev. D **85**, 125027 (2012).

[48] G. Aslanyan, L. C. Price, J. Adams, T. Bringmann, H. A. Clark, R. Easther, G. F. Lewis, and P. Scott, Ultracompact Minihalos as Probes of Inflationary Cosmology, Phys. Rev. Lett. **117**, 141102 (2016).
[49] T. Nakama, T. Suyama, K. Kohri, and N. Hiroshima, Constraints on small-scale primordial power by annihilation signals from extragalactic dark matter minihalos, Phys. Rev. D **97**, 023539 (2018).
[50] B. J. Carr, K. Kohri, Y. Sendouda, and J. Yokoyama, New cosmological constraints on primordial black holes, Phys. Rev. D **81**, 104019 (2010).
[51] M. S. Delos, A. L. Erickcek, A. P. Bailey, and M. A. Alvarez, Are ultracompact minihalos really ultracompact?, Phys. Rev. D **97**, 041303 (2018).
[52] M. S. Delos, A. L. Erickcek, A. P. Bailey, and M. A. Alvarez, Density profiles of ultracompact minihalos: Implications for constraining the primordial power spectrum, Phys. Rev. D **98**, 063527 (2018).
[53] J. Adamek, C. T. Byrnes, M. Gosenca, and S. Hotchkiss, WIMPs and stellar-mass primordial black holes are incompatible, Phys. Rev. D **100**, 023506 (2019).
[54] A. Belikov and J. Silk, Diffuse gamma ray background from annihilating dark matter in density spikes around supermassive black holes, Phys. Rev. D **89**, 043520 (2014).
[55] T. Lacroix and J. Silk, Intermediate-mass black holes and dark matter at the galactic center, Astrophys. J. Lett. **853**, L16 (2018).
[56] J.-G. Cheng, S. Li, Y.-Y. Gan, Y.-F. Liang, R.-J. Lu, and E.-W. Liang, On the gamma-ray signals from UCMH/mini-spike accompanying the DAMPE 1.4 TeV e^+e^- excess, Mon. Not. R. Astron. Soc. **497**, 2486 (2020).
[57] Z.-Q. Xia, Z.-Q. Shen, X. Pan, L. Feng, and Y.-Z. Fan, Investigating the dark matter minispikes with the gamma-ray signal from the halo of M31, arXiv:2108.09204.
[58] G. Ambrosi *et al.* (DAMPE Collaboration), Direct detection of a break in the teraelectronvolt cosmic-ray spectrum of electrons and positrons, Nature (London) **552**, 63 (2017).
[59] X.-J. Huang, Y.-L. Wu, W.-H. Zhang, and Y.-F. Zhou, Origins of sharp cosmic-ray electron structures and the DAMPE excess, Phys. Rev. D **97**, 091701 (2018).
[60] Y. Zhao, X.-J. Bi, S.-J. Lin, and P.-F. Yin, Nearby dark matter subhalo that accounts for the DAMPE excess, Chin. Phys. C **43**, 085101 (2019).
[61] J. A. Fillmore and P. Goldreich, Self-similar gravitational collapse in an expanding universe, Astrophys. J. **281**, 1 (1984).
[62] E. Bertschinger, Self-similar secondary infall and accretion in an Einstein-de Sitter universe, Astrophys. J. Suppl. Ser. **58**, 39 (1985).
[63] M. Vogelsberger, S. D. M. White, R. Mohayaee, and V. Springel, Caustics in growing cold dark matter haloes, Mon. Not. R. Astron. Soc. **400**, 2174 (2009).
[64] A. D. Ludlow, J. F. Navarro, V. Springel, M. Vogelsberger, J. Wang, S. D. M. White, A. Jenkins, and C. S. Frenk, Secondary infall and the pseudo-phase-space density profiles of cold dark matter haloes, Mon. Not. R. Astron. Soc. **406**, 137 (2010).
[65] P. Ullio, L. Bergström, J. Edsjö, and C. Lacey, Cosmological dark matter annihilations into γ rays: A closer look, Phys. Rev. D **66**, 123502 (2002).
[66] M. Cirelli, G. Corcella, A. Hektor, G. Hütsi, M. Kadastik, P. Panci, M. Raidal, F. Sala, and A. Strumia, PPPC 4 DM ID: A poor particle physicist cookbook for dark matter indirect detection, J. Cosmol. Astropart. Phys. 03 (2011) 051.
[67] L. Bergström, J. Edsjö, and P. Ullio, Spectral Gamma-Ray Signatures of Cosmological Dark Matter Annihilations, Phys. Rev. Lett. **87**, 251301 (2001).
[68] G. Steigman, B. Dasgupta, and J. F. Beacom, Precise relic WIMP abundance and its impact on searches for dark matter annihilation, Phys. Rev. D **86**, 023506 (2012).
[69] A. Domínguez *et al.*, Extragalactic background light inferred from AEGIS galaxy-SED-type fractions, Mon. Not. R. Astron. Soc. **410**, 2556 (2011).
[70] Y. Inoue, S. Inoue, M. A. R. Kobayashi, R. Makiya, Y. Niino, and T. Totani, Extragalactic background light from hierarchical galaxy formation: Gamma-ray attenuation up to the epoch of cosmic reionization and the first stars, Astrophys. J. **768**, 197 (2013).
[71] C. Gruppioni *et al.*, The Herschel PEP/HerMES luminosity function. I: Probing the evolution of PACS selected galaxies to $z\tilde{}4$, Mon. Not. R. Astron. Soc. **432**, 23 (2013).
[72] H. Chernoff, On the distribution of the likelihood ratio, Ann. Math. Stat. **25**, 573 (1954).
[73] Q. Yuan *et al.*, Interpretations of the DAMPE electron data, arXiv:1711.10989.
[74] J. Cao, L. Feng, X. Guo, L. Shang, F. Wang, and P. Wu, Scalar dark matter interpretation of the DAMPE data with U(1) gauge interactions, Phys. Rev. D **97**, 095011 (2018).
[75] X. Pan, C. Zhang, and L. Feng, Interpretation of the DAMPE 1.4 TeV peak according to the decaying dark matter model, Sci. China Phys. Mech. Astron. **61**, 101006 (2018).
[76] T. Ghosh, J. Kumar, D. Marfatia, and P. Sand ick, Searching for light from a dark matter clump, J. Cosmol. Astropart. Phys. 08 (2018) 023.
[77] K. Belotsky, A. Kamaletdinov, M. Laletin, and M. Solovyov, The DAMPE excess and gamma-ray constraints, Phys. Dark Universe **26**, 100333 (2019).
[78] R. Catena and P. Ullio, A novel determination of the local dark matter density, J. Cosmol. Astropart. Phys. 08 (2010) 004.
[79] A. M. Atoyan, F. A. Aharonian, and H. J. Völk, Electrons and positrons in the galactic cosmic rays, Phys. Rev. D **52**, 3265 (1995).